Available online at www.sciencedirect.com
SCIENCE DIRECT®
PERGAMON
Electrochimica Acta 48 (2003) 1845–1859
ELECTROCHIMICA Acta
www.elsevier.com/locate/electacta

Oxygen permeation studies on alternative proton exchange membranes designed for elevated temperature operation

Lei Zhang, Chengsong Ma, Sanjeev Mukerjee *

Department of Chemistry, Northeastern University, 360 Huntington Avenue, Boston, MA 02115, USA

Received 4 November 2002; received in revised form 17 March 2003; accepted 19 March 2003

Abstract

Kinetic and mass transport properties were investigated for the oxygen reduction reaction in Nafion 117 and a sulfonated poly (arylene ether sulfone) membrane (SPES-40, 40% sulfonated groups/repeat unit) under 1 atm oxygen pressure, 100% relative humidity in a temperature range of 303–343 K using a solid-state electrochemical cell. Kinetic parameters were obtained using slow-sweep voltammetry while mass transport parameters, the diffusion coefficient (D) and solubility (C), were obtained using chronoamperometry at a Pt (microelectrode)/proton exchange membrane (PEM) interface. Oxygen reduction kinetics was found to be similar for both Nafion® 117 and SPES-40 membrane at the Pt microelectrode interface. The temperature dependence of O_2 permeation parameters showed same trends for both the membranes studied, there was an increase in D and a concomitant decrease in C. Despite lower equivalent weight and hence higher water content SPES-40 exhibited relatively close values of D with Nafion® 117. The results are discussed in the context of their different microstructures. Values of C showed a closer relationship to water content and the percent volume of aqueous phase in the respective membranes. The values of overall oxygen permeability were significantly higher in Nafion® 117, with a higher positive slope in its variation with temperature.
© 2003 Elsevier Science Ltd. All rights reserved.

Keywords: Sulfonated poly(arylene ether sulfone); O_2 Diffusion coefficient; O_2 Solubility; O_2 Permeability; Microelectrode

1. Introduction

Proton exchange membrane fuel cells (PEMFC) are promising power sources for vehicular transportation, residential and consumer electronics [1]. Amongst the key components is the polymer electrolyte membrane (PEM) that provides the ionic pathway and acts as a gas separator. The current state-of-the-art is based on perfluorinated sulfonic acid chemistry, such as those from Dupont (Nafion®), Asahi chemicals (Aciplex®) and others. These achieve good performance when operating at 80–90 °C and high relative humidity (> 80% RH) [2–4]. They have good mechanical strength, chemical stability and high proton conductivity [1]. However, these membranes remain expensive and have several limiting factors such as low conductivity at low RH [5], high methanol permeability [6,7], and a low T_g (glass transition temperature) [8] which restricts its application to below 100 °C.

Transitioning to temperatures above 100 °C provides for several attractive options which include higher CO tolerance [9,10], better water and heat management related to interfacing fuel cells with other system components such as the fuel processor unit.

Alternative hydrated membranes to the perfluorinated sulfonic acid based systems (such as Nafion®) possessing high proton conductivity at lower RH and stability at elevated temperatures are currently the focus of a lot of research and development. Most of them are based on engineering polymers with high thermo-chemical stability [11], typically with a high degree of aromatic character, where the monomer consists of a variety of fused phenyl rings linked together with a number of bridging moieties (hereafter referred to as membranes with aromatic backbone). Sulfonation of these materials involves either using sulfonated monomer in the polymer synthesis or using a variety of methods for post-sulfonation. Several families of poly-

* Corresponding author. Tel.: +1-617-373-2382; fax: +1-617-373-8795.
E-mail address: smukerje@lynx.ncu.edu (S. Mukerjee).

0013-4686/03/$ - see front matter © 2003 Elsevier Science Ltd. All rights reserved.
doi:10.1016/S0013-4686(03)00257-3

mers have been developed in this context, these include sulfonated poly ether (ether) ketone (SPEEK) [12–15], polyimides [16], poly ether sulfone (SPES),[17–19] poly sulfide sulfone (SPSS) [20,21], poly phenyl quinoxaline (SPQQ) [22], aryl oxyphosphazene (SAOP) [23], propylated poly (benzimidazole) [24–26] and poly (phenylene sulfide sulfone) [27].

In this search for elevated-temperature PEM's, sulfonated poly (arylene ether sulfone) (SPES) family have recently been reported as promising candidate material [28–32]. Being well-known engineering thermoplastics, poly (arylene ether sulfones) (Structure 1) displays a high glass transition temperature (T_g) of 195 °C, good resistance to hydrolysis and oxidation, excellent mechanical properties and high thermal stability [33]. The closely related sulfonic acid systems such as Nafion®. Their use as the ion conducting components in PEM fuel cells operating at elevated temperature not only requires excellent proton conduction at elevated temperatures, preferably at low RH but also compatible reactant transport characteristics. For an electrochemical charge transfer to be successful only the dissolved reactant moieties are relevant, therefore efficient transport of reactant species such as oxygen within the electrolyte is crucial. This efficient reactant transport or permeation comprises of two important components, solubility (C), and diffusion coefficient (D). Together, they determine the crossover of gases across the membrane thus affecting the open circuit potential and more importantly, they determine the availability of the reactant at the electrocatalyst–electrolyte interface. This is most important, in determining the onset of mass transport limitations in a typical fuel cell performance.

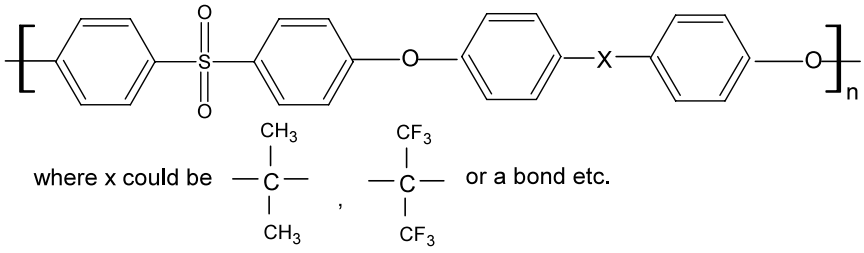

(1)

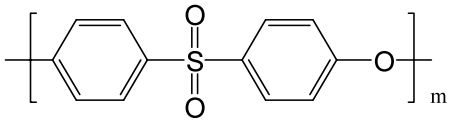

(2)

Poly ether sulfone (Structure 2) is totally devoid of aliphatic hydrocarbon groups and exhibit even higher thermal stability ($T_g = 230$ °C) [34]. Sulfonation of these poly (arylene ether sulfone) leading to formation of a practical proton exchange membrane for fuel cell application is therefore a strong motivator for use of these macromolecules for elevated temperature operation. Recently, direct polymerization using sulfonated monomers have been reported by the Virginia Polytechnic Institute and State University [30,31,35–37]. Polyarylene ether sulfone (referred to by Virginia Tech., group as PBPSH-XX) copolymers with high sulfonation levels ($XX = 40$–60, where XX represents the fraction of the sulfonated component in these copolymers), have shown proton conductivity in excess of 0.08 S cm^{-1} (at room temperature), which meets the requirement for high-performance PEMFC [38].

These membranes however represent very different chemistry relative to the conventional perfluorinated

In a typical PEM fuel cell, the electrode–electrolyte interface comprises of the 'membrane electrode assembly' (MEA), which is a hot-pressed composite structure. The overpotentials for activation, ohmic and mass transport are kept low by specially formulating the electrode structure and the hot pressing conditions so as to maximize the gas transport and mobility of electrons and ions. This is typically done using a multilayer electrode structure where the substrate is a carbon cloth or paper in contact with the bipolar plate. This substrate is coated with a layer of teflonized carbon, which is commonly referred to as the gas diffusion layer. The charge transfer interface with the membrane is called the 'reaction layer'. It is typically a thin layer of catalyst and ionomer (in most cases the ionomer is a solubilized form of the electrolyte membrane) with or without a binder such as Teflon, deposited on top of the teflonized carbon layer. This reaction layer therefore extends the charge transfer interface from the membrane surface deeper into the electrode structure in order to increase the interfacial area available to carry out the desired reaction. It is in this reaction layer, where the transport of dissolved gases to the electrocatalyst interface occurs,

which is determined by the permeation capability of the surrounding ionomer.

ORR is well known as a source of inefficiency in fuel cell reaction and is a common denominator for reformer based and direct methanol fuel cells. Studies on oxygen electrodes typically show three distinct regions in the cathode polarization curve. At low current densities, the exponential drop of potential away from the reversible potential of oxygen electrode (1.23 V vs. RHE at STP) is referred as activation loss, this is ascribed to sluggish kinetics of the oxygen reduction reaction. The reactant gas solubility and the intrinsic electrocatalytic properties of the electrolyte in contact with the Pt catalyst at the reaction layer of the electrode control the electrocatalytic efficiency of the reactions. At intermediate current densities, the linear potential drop is due to ohmic effect. The proton-conducting properties of the bulk electrolyte and the internal resistances of fuel cell determine this ohmic contribution. At high current densities, the sharp drop of the potential is due to the insufficient supply of reactant gases to the cathode catalyst sites. Modeling calculations have demonstrated that the oxygen permeability (product of solubility and diffusivity) determine the mass-transport rates at the cathode [39]. Therefore, in addition to the effort of increasing the proton conductivity of the membranes to reduce the ohmic contribution, research on the kinetics and reactant permeation properties is extremely important for minimizing the activation and mass-transport limitation.

In previous publications, investigations of oxygen reduction reaction at Pt and liquid electrolyte interface such as phosphoric acid has been performed under a variety of conditions [40–44]. Various methods such as microelectrode technique [45–51], electrochemical monitoring technique (EMT) [52–56], and gas chromatography [57–59] have been used for gas permeation measurements. Mass transport parameters for oxygen reduction reaction at the interface between Pt and a variety of solid-state perfluorosulfonic acid-type materials (Nafion® and Aciplex® membranes) have been studied intensively since the pioneering work of Parthasarathy et al. [45]. Prior studies on these membranes investigating oxygen transport characteristics have examined the effect of both environmental (temperature and pressure) [46,47,49] and membrane structural composition (equivalent weight) [48]. Similar investigations had been made on a series sulfonated α,β,β-trifluorostyrene (BAM®, Ballard, Canada) membranes and sulfonated styrene-(ethylene-butylene)-styrene triblock copolymers (DAIS®, DAIS-Analytic, USA) by Holdcroft and co-workers [49–51]. These studies suggested that oxygen transport behavior was primarily related to water content in the PEM. The effect of increase in equivalent weight [51] was shown to cause a decrease in diffusion coefficient of oxygen and increase in the solubility.

This investigation aims to evaluate SPES membranes as candidate electrolyte for PEMFC by investigating their oxygen permeation characteristics and interfacial kinetics. For this a solid state microelectrode technique is employed, which is used to determine the kinetic and mass transport parameters (solubility and diffusivity) for O_2 reduction reaction at Pt micro-electrode/membrane interface. Slow-sweep voltammetry and chronoamperometry measurements were conducted as a function of temperature at ambient pressure conditions. The kinetic parameters, O_2 diffusion coefficient and solubility values obtained were compared with corresponding values for a Nafion® 117 membrane (control experiment). All values in this investigation pertain to measurements at 1 atm pressure (ambient pressure). This was motivated by our desire to measure these parameters without any interference of pressure, this also forms the first time when such measurements are reported at ambient pressure conditions.

2. Experimental

2.1. Membranes

Two membranes were studied in this investigation. Poly (arylene ether sulfone) membrane with Structure (3), containing two sulfonate groups per repeat unit were prepared at Virginia Polytechnic and State University (Professor James McGrath's group). This synthesis involved potassium carbonate mediated direct aromatic nucleophilic substitution polycondensation of disodium 3,3′-disulfonate-4,4′-dichlorodiphenyl sulfone (SDCDPS), 4,4′-dichlorodiphenylsulfone (DCDPS) and 4,4′-diphenol. Detailed preparation methodology, reaction conditions and membrane properties, such as T_g,

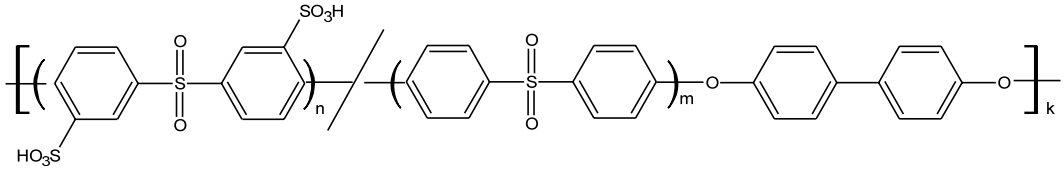

(3)

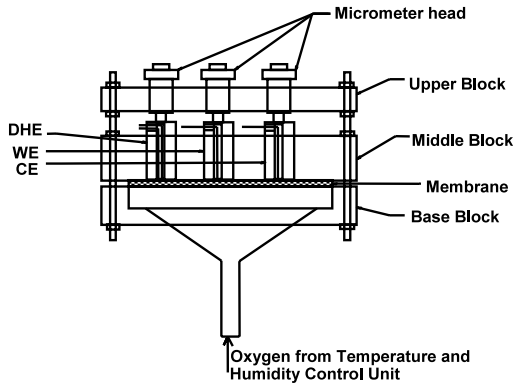

Fig. 1. Schematic of the solid state electrochemical cell with the working electrode as a 100-μm Pt wire (WE), a dynamic hydrogen reference electrode (DHE) and a Pt plug counter electrode (CE).

hydrophilicity, viscosity, TGA, AFM (hydrophilic domain size, phase inversion) and proton conductivity are reported elsewhere [38]. The polymer used in this investigation was a 40:60 ratio in terms of SDCPDS/DCDPS (100n/n+m, Structure (3)). This polymer, referred to as PBPSH-40 by the Virginia Tech., group, is referred to as SPES-40 in this paper. Nafion® 117 (Dupont) was bought from a commercial vendor (Aldrich chemicals). Chemical structure of this material is illustrated in Structure (4).

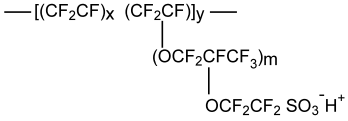

(4)

Membranes were boiled in 1 M sulfuric acid for 2 h and then soaked for 48 h in 1 M sulfuric acid at room temperature to ensure full protonation. After protonation, the membranes were rinsed several times and stored in deionized water.

Measurements of water uptake followed typical methods reported earlier [51]. Membranes were initially dried at 80 °C in a vacuum oven, overnight (12 h). The membranes were then equilibrated by immersing them in an enclosed water container, which was placed in a constant temperature oven. Following equilibration for 4–6 h, the membranes were quickly weighed, taking care that excess water was removed prior to weighing. This allowed measurement of water uptake as a function of temperature. The water content in terms of wt.% was determined according to: $H_2O[\%] = [(\text{wet weight} - \text{dry weight})/\text{dry weight}] \times 100\%$. Number of moles of water per sulfonic acid group ($\lambda = [H_2O]/SO_3^-$) was also calculated.

2.2. Electrodes

The working electrode was a 100 μm diameter Pt microelectrode (Bio Analytical Systems, BAS, West Lafayette, IN). The surface of the microelectrode was polished with 5, 3 and 1 μm diamond polish solutions (BAS-polishing kit) and finally with 0.05 μm alumina polish (BAS). Following the polishing step, the electrode was sonicated in deionized water for 60 s and rinsed, it was stored in deionized water before assembling into the solid state microelectrode cell. A solid-state dynamic hydrogen electrode (DHE) served as the reference electrode. It was constructed by sealing two 0.25 mm diameter Pt wires (Alfa Aesar) in a double-bore glass tube. Prior to each experiment, the electrodes were platinized using a 20 mM chloroplatinic acid solution. A 9 V battery in series with a 2.2 MΩ resistor was used for constant current supply between the two platinized electrodes in the DHE in contact with the hydrated membrane. The counter electrode was a 1.6 mm diameter Pt electrode (BAS) spot-welded to a $5 \times 5 \times 0.01$ mm^3 (thick) Pt foil.

2.3. Solid-state electrochemical cell setup

A new cell was designed to perform solid-state electrochemical experiments under controlled temperature and RH. A schematic of the cell is given in Fig. 1. The apparatus consisted of three Teflon blocks. The bottom Teflon block housed a glass base with a built in fritted glass filter (47 mm diameter, Millipore), which had a porous and smooth flat surface to support the membrane of interest. The bottom end of the glass filter base was connected to the gas supply through a swagelock adapter. This swagelock adapter had arrangements for sealed thermocouple and humidity sensor attachments. This enabled measurement of inlet gas temperature and humidity immediately below the membrane electrode interface. The middle Teflon block had three through holes to fit in the working, counter and reference electrodes. This was used to provide conduit for the wires connecting these electrodes. The upper stainless steel block contained three flat-tip micrometer heads. By screwing forward its spindle, the micrometer head was capable of applying variable pressure to the electrode–membrane contact. Four screw rods and several nuts hold the three blocks tightly together. A thermocouple (Omega engineering, CT) was inserted into the cell from the bottom with its tip touching the membrane. Temperature control was achieved by using a temperature controller (Watlow, series-965).

The overall set up of this electrochemical cell was based on earlier designs [45–47]. In our set up all the electrodes were on the same side of the membrane, instead of having the membrane sandwiched between the working electrode on one side and counter and reference electrode on the other. The modification in our set up ensured good mechanical contact at membrane–electrode interface. This was achieved using micrometer

heads, which could be more conveniently used to adjust the clamping pressure as compared to springs in previous cell setups [45–47]. In this arrangement the distance between the working and the reference electrode were similar to those in previous setups [45]. The impedance between working and reference electrodes was monitored and standard iR correction methods applied (Echochemie, model AUTOLAB PGSTAT 30).

During the experiment, the cell was put into a modified constant temperature oven, which provided a constant cell temperature and served as a Faraday cage. Gas was supplied using a special heating and humidity control unit. This set up, built in-house, comprised of a humidification unit, which was a temperature-controlled bubbler. Humidified gas from this unit was mixed with a controlled amount of dry gas using a system of two mass flow controllers interfaced with a computer with Labview (National Instruments) software control. Adjustments to the bubbler temperature and relative flow rates of the dry and wet gas enabled the control of humidification of the gas at the inlet of the solid state microelectrode set up. All results reported in this paper are at 100% RH, hence there was no dry gas input used for our experiments. All experiments were conducted at ambient pressure, with the humidification bottle temperature at least 10 °C higher than the cell temperature. The RH was independently measured using a humidity sensor (ELECTRONIK, series EE-30) at the bottom of the solid-state microelectrode assembly. The flow rate of the humidified gas entering the cell was set at about 600 ml min^{-1}. A higher or lower flow rate was found to have the potential of causing flooding or drying inside the cell.

2.4. Electrochemical techniques and instrumentation

A computer controlled digital potentiostat/galvanostat (Autolab model, PGSTAT-30) was employed to conduct cyclic voltammetry, slow-sweep voltammetry and chronoamperometry experiments. All potentials stated here are relative to DHE.

Cyclic voltammetry (scan rate = 50 mV s^{-1}) in the potential range 0.08–1.5 V in nitrogen was carried out for evaluating the electrochemically active area and roughness factors of Pt microelectrode. Fast scan cyclic voltammetry (0.08–1.5 V) in oxygen at a scan rate of 100 mV s^{-1} was performed during the equilibrium periods at each temperature for cleaning and activating the Pt micro-working electrode.

Slow-sweep voltammograms between 1.2 and 0.3 V at 2 mV s^{-1} scan rate were recorded to determine the limiting current I_d, which is given by Eq. (1):

$$I_d = n\pi FDCr \tag{1}$$

where $n = 4$, referring to the number of electrons transferred per mol of oxygen in the overall O_2 reduction at Pt electrode ($O_2 + 4e^- + 4H^+ \rightarrow 2H_2O$), F is Faraday's constant, D is the diffusion coefficient of O_2, C is the solubility of O_2 and r is the radius of the Pt microelectrode. Electrode kinetic parameters were obtained using slow scan voltammograms. For this the mass transport corrected Tafel equation was used:

$$\eta = \frac{2.303RT}{\alpha nF}\log i_0 + \frac{-2.303RT}{\alpha nF}\log\left[\frac{i_d i}{i_d - i}\right] \tag{2}$$

where, η is the overpotential ($E - E^\circ$), R is the gas constant, T is the absolute temperature, α is the transfer coefficient, n is the number of electrons involved in the rate determining step of O_2 reduction on Pt ($H_3O^+ + O_2 + e^- \rightarrow O_2H_{(ads)} + H_2O$), i_0 is the exchange current density, i_d is the limiting current density, and i is the current density. The activation energy for oxygen reduction reaction was obtained from Arrhenius plots of log i_0 versus $10^3 T^{-1}$ based on Eq. (3).

$$E_a = -2.303R\left[\frac{d\log i_0}{d(1/T)}\right] \tag{3}$$

Chronoamperometry experiment was used to determine diffusion coefficient and solubility of oxygen. It was performed by holding the potential of the microelectrode at 1.2 V for 20 s and then stepping to 0.4 V for 5 s. Plotting of current, I, versus reciprocal of the square root of time, $t^{-1/2}$, for a time domain from 1 to 5 s gave linear relationship corresponding to the modified *Cottrell* Eq. (4):

$$I(t) = \frac{nFAD^{1/2}C}{\pi^{1/2}t^{1/2}} + \pi FnDCr \tag{4}$$

where, A is the geometric area of the microelectrode. D and C values were obtained simultaneously from linear regression analysis of the slope and intercept. For details on the choice of this equation and use of this methodology see Refs. [45–47,49]. The activation energy of O_2 diffusion and enthalpy of dissolution of O_2 in the membranes were calculated according to Eqs. (5) and (6).

$$E_d = -2.303R\left[\frac{d\log D}{d(1/T)}\right] \tag{5}$$

$$\Delta H_s = -2.303R\left[\frac{d\log C}{d(1/T)}\right] \tag{6}$$

2.5. Experimental procedure

After incorporation into the cell, the membrane was equilibrated with humidified gas at 30 °C for at least 12 h. Electrochemical measurements were conducted at 100% RH in a temperature range of 30–70 °C and 1 atm pressure. Series of electrochemical measurements for

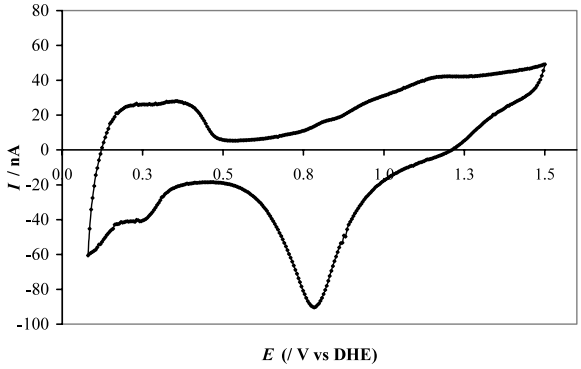

Fig. 2. Representative plot of the cyclic voltammogram at a Pt/SPES-40 interface under conditions of 100% RH, 313 K, 1 atm N_2 pressure. Scan rate = 50 mV s^{-1}.

determining both interfacial kinetics and mass transport parameters were made at each temperature after equilibration for at least 2 h. The choice of 1 atm in contrast to higher pressures used in previously reported investigations was due to the fact that modification of our experimental set up allowed very high reproducibility at ambient pressure conditions. This is in contrast to earlier efforts where at least 2 atm was necessary for getting reasonable data quality. One atmosphere (ambient pressure) was chosen as it provided a good baseline to investigate the effect of change of temperature, without interference from pressure effects. All experiments conducted for each of the membranes were repeated at least three times and the reproducibility monitored. For the kinetic and mass transport measurements very good reproducibility was obtained as discussed in Section 3.

3. Result and discussion

3.1. Cyclic voltammogram at Pt/PEM interface

Cyclic voltammetry (CV) was used to determine qualitatively the nature of the interfacial contact between the Pt microelectrode and the hydrated membrane. Uncompensated resistance at the membrane electrode interface can shift the oxygen reduction wave to more negative potentials [45] which can constitute a potential source of error in determination of the kinetic and mass transport parameters. To minimize the effect of variability in contact resistance, the position of the micrometer heads were adjusted until the contact impedance stopped changing. One of the most convenient methods to detect this was to monitor the shift in the oxide reduction peak. For this, the working electrode was exposed to an inert gas (N_2) under 100% relative humidification conditions at a temperature of 40 °C. When no further positive shifts in the oxide reduction peak were observed as a function of change in contact pressure of the working electrode and electrolyte membrane, the micrometer was locked into position. Fig. 2 gives an example of CV recorded under appropriate clamping pressure obtained at Pt/SPES-40 interface at 40 °C. All the Pt surface electrochemical features are clearly resolved in this voltammogram. In addition, the impedance of the working electrode relative to the reference was monitored as a function of the micrometer head positions (contact pressure) until they stopped changing; this corresponded well with the shifts in the oxide reduction peak.

Table 1
Real areas obtained from the charge under the hydrogen adsorption and desorption regions (average value) in the cyclic voltammogram and corresponding roughness factors for the various Pt/PEM systems studied

Interface	Real area (cm^2)	Roughness factor
Pt/0.5M H_2SO_4	7.72×10^{-4}	9.84
Pt/SPES-40	7.41×10^{-4}	9.44
Pt/Nafion 117	7.45×10^{-4}	9.48

Well-resolved CVs obtained at Pt/PEM interfaces were used to evaluate the electrochemically active area and roughness factor of the microelectrode. Details of the calculations are reported elsewhere [60]. By averaging the area under hydrogen adsorption and desorption waves and taking into account the double-layer charging area (assuming 210 μC cm^{-2} for a smooth Pt surface [61]), the electrochemically active area of the microelectrode at the interface with the membrane was found to be about nine times larger than its geometrical area (Table 1). The real areas and roughness factors obtained in this solid-state cell were comparable to those obtained in Pt/0.5 M H_2SO_4 (Table 1). This is evidence of good contact between the working electrode and the membranes. These values also compared well with previously reported roughness factors [45,62]. It is also important to point out that the results reported in Table 1, are an average of three separate experiments conducted under the same conditions. The deviations in the data were less than 3%.

Fast-scan CV (100 mV s^{-1}, in the range 0.08–1.5 V) under oxygen flow at 100% RH was routinely carried out in this work during the periods of cell equilibration at each temperature, this helped in cleaning the microelectrode.

3.2. Determination of electrode kinetic parameters at a Pt/PEM interface by slow-scan voltammograms

All potentials reported in this work are with respect to DHE. It is well recognized that correction of this reference potential with respect to the standard hydrogen electrode (SHE) reference potential provides a more accurate picture of the absolute values of exchange

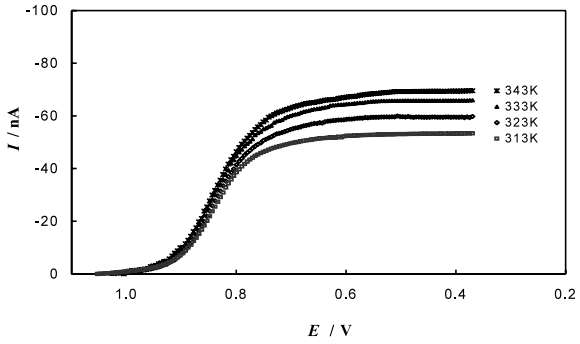

Fig. 3. Representative plot showing a slow-sweep voltammogram for O_2 reduction at the Pt/SPES-40 interface under conditions of 100% RH, in the temperature range 313–343 K, 1 atm O_2 pressure; scan rate = 50 mV s^{-1}.

current densities. However, the reference potential for DHE shows variations as a function of temperature and pressure [63]. Hence using a correction term determined at one condition such as those reported earlier [49] (a correction of -80 ± 10 mV, with respect to a Calomel electrode measured in 0.5 M H_2SO_4 at room temperature), is not expected to hold in the entire temperature range [63]. Since the purpose here is to compare the kinetics of ORR at a Pt microelectrode-membrane interface, shifts from absolute values for exchange current densities were neglected. Comparison of all kinetic measurements with respect to DHE provided a more stable and accurate comparison at different membrane interfaces.

Evaluation of electrode kinetics of O_2 reduction at Pt/Nafion® 117 interface as a function of temperature had been discussed in great detail elsewhere [46,49]. Briefly, slow sweeping (2 mV s^{-1}) the potential of working electrode at O_2-equilibrated membrane gives rise to sigmoidal-shaped voltammograms. The diffusion-controlled region of these pseudo-steady-state curves provided the magnitudes of limiting current (I_d). The activation-controlled regions were used to generate

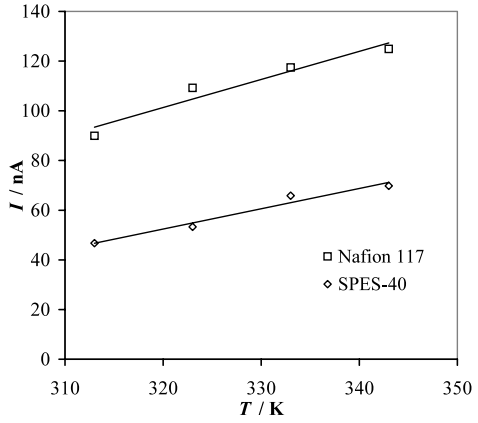

Fig. 4. Plots of limiting current, I_d, versus temperature for Pt/PEM systems studied under conditions of 100% RH, as a function of temperature (313–343 K), 1 atm O_2 pressure.

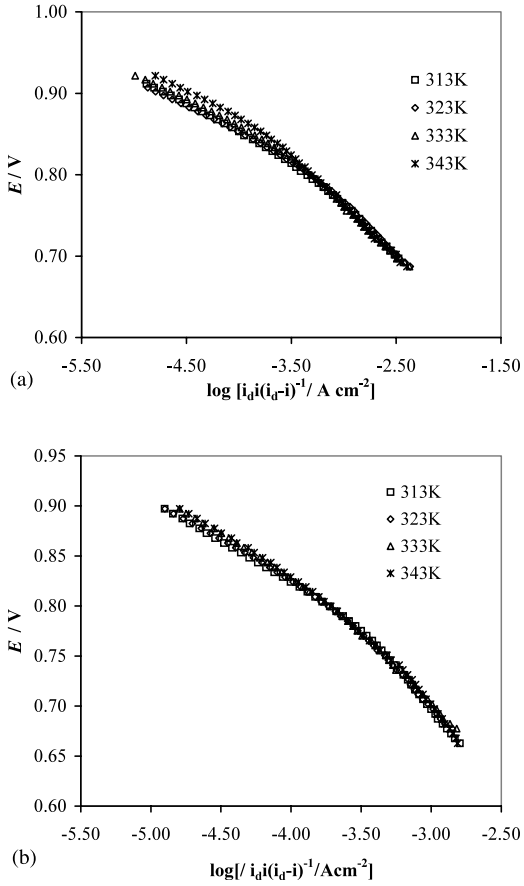

Fig. 5. Plots of mass-transport corrected Tafel plots for: (a) Nafion 117; (b) SPES-40 membrane under conditions of 100% RH, as a function of temperature in the range 313–343 K, 1 atm O_2 pressure.

quantitative data for O_2 reduction kinetics via mass-transport corrected Tafel analysis.

Fig. 3 shows representative slow sweep voltammograms as a function of temperature in the range 40–70 °C, at a Pt/SPES-40 interface. As expected, the oxygen reduction waves are shifted away from the theoretical reversible potentials E_r because of the poor reaction kinetics. The limiting current associated with the reduction reaction displays an increasing trend with temperature. Plots of I_d versus temperature for the two membranes are shown in Fig. 4. Nafion® 117 exhibited significantly higher I_d over the whole temperature range as compared to SPES-40. According to Eq. (1), the product of D and C affects the magnitude of I_d. Different I_d values therefore suggest that their corresponding O_2 permeability ($D \times C$) would also be different. This will be discussed in more detail later.

Previous investigations on Pt/liquid acid electrolytes [64,65] as well as Pt/ Nafion® 117 interface [45,49] have shown the existence of two regions in the mass transport corrected Tafel plots. The two sets of Tafel kinetic parameters at low and high current density regions correspond to the oxygen reduction reaction at oxide-covered and oxide-free surface of Pt. Tafel plots for

Table 2
Electrode kinetic parameters for various PEM systems at the interface with a Pt micro-wire (100 μm) working electrode, studied as a function of temperature in the range 313–343 K, under conditions of 100% RH, 1 atm O_2 pressure

Membrane	T (K)	E_r (V) vs. SHE	Slope (lcd) mV per decade	i_0 (lcd) A cm^{-2}	α (lcd)	Ea (lcd) kJ mol^{-1}	Slope (hcd) mV per decade	i_0 (hcd) A cm^{-2}	α (hcd)	Ea (hcd) kJ mol^{-1}
Nafion® 117	313	1.213	−70.0	7.10E−10	0.89	44.88	−117.1	1.39E−7	0.53	32.2
	323	1.204	−72.3	1.27E−9	0.89		−117.2	1.77E−7	0.55	
	333	1.196	−71.5	1.88E−9	0.92		−120.9	2.58E−7	0.55	
	343	1.188	−71.4	3.33E−9	0.95		−125.6	4.10E−7	0.54	
SPES-40	313	1.213	−83.7	2.20E−9	0.74	46.74	−144.4	2.41E−7	0.44	25.8
	323	1.204	−85.4	3.47E−9	0.75		−145.4	3.17E−7	0.45	
	333	1.196	−88.3	7.22E−9	0.74		−148.0	3.71E−7	0.45	
	343	1.188	−88.7	9.85E−9	0.77		−148.7	6.02E−7	0.45	

Note: All current densities were calculated relative to the real area of the working electrode. E_r at different temperatures was calculated according to Ref. [49].

Nafion® 117 (Fig. 5(a)) and SPES-40 (Fig. 5(b)) show the two well-defined linear regions similar to those reported earlier [45].

Table 2 lists the calculated kinetic parameters based on mass transport corrected Tafel equation. Comparison of the exchange current density for both the membranes in the low current density (lcd) and high current density (hcd) regions, exhibited approximately the same order of magnitude, although SPES-40 membrane showed slightly higher values than Nafion® 117. The Tafel slopes for all the membranes studied show deviations from the 'typical' number of −60 mV per decade [64] (lcd) and −120 mV per decade [65] (hcd). Further, the transfer coefficient α also exhibited some deviations from the characteristic value of 1 (lcd) and 0.5 (hcd). For example, the Tafel slopes for SPES 40 at low and high current regions ranged from −83.7 to −88.7 mV per decade and −144.4 to −148.7 mV per decade; its α values at lcd ranged around 0.74–0.77. Such deviations of Tafel parameters from typical values are inherent in these measurements as evident from similar results on Nafion® 117, reported [45] earlier. The exact cause is complex and difficult to control, Beattie et al. [49] had suggested that impurities in the membranes could be a significant contributor.

Unlike previous report [46], there was no correlation found between α and temperature in the high current density region (oxide free region) for Nafion® 117 and SPES-40 membrane. No such correlation with Nafion® 117 was also observed by Beattie et al. [49]. An increase in the symmetry factor (α) with temperature has been interpreted in terms of Bokris–Gochev theory [66]. According to this theory, based on investigation at a Pt/trifluoro methane sulfonic acid (TFMSA) interface, at potentials greater than the potential of zero charge, the excess positive charge on the electrode is balanced by the negatively charged sulfonic acid groups in the electrolyte. Since these sulfonate anions are enclosed within the hydrophilic domains of the micelles formed by perfluorinated sulfonic acids such as TFMSA, some of the water molecules in the aqueous domains interact with the SO_3^- via hydrogen bonding. The anomalous dependence of symmetry factor (α) with temperature has been ascribed to changes in the hydrogen bonding with temperature.

The activation energies of oxygen reduction reaction, E_a (kJ mol^{-1}), are also listed in Table 2. For all the membranes, the activation energies in lcd are higher than in hcd as noted previously by Parthasarthy et al. [46]. As reported previously by Sepa et al. [67], based on both experimental results and theoretical calculations, the difference between the activation energies in the lcd (oxide covered) and hcd (oxide free) regions should be 16 kJ mol^{-1}. This is based on the assumption that the first electron transfer step in both the regions is the rate determining step in accordance to the equation: O_2+

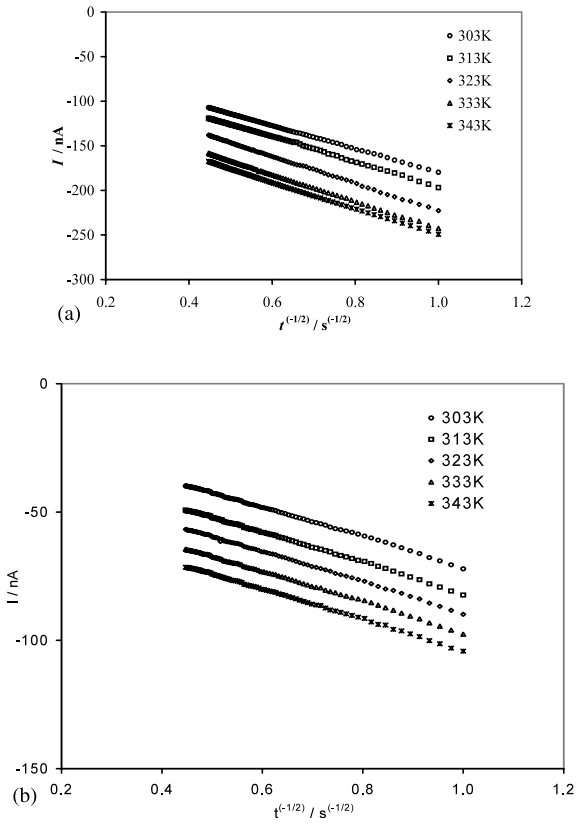

Fig. 6. Plots of current, I versus $t^{-1/2}$ (time$^{-1/2}$) for O_2 reduction at: (a) Pt/ Nafion® 117; and (b) Pt/SPES-40 interface under conditions of 100% RH, temperature in the range of 303–343 K and 1 atm O_2 pressure.

$H^+ + e^- \rightarrow O_2H_{ads}$. Our results show a difference of 12.68 kJ mol^{-1}for Nafion® 117 and 20.94 kJ mol^{-1} for SPES-40. Within the limits of error inherent in these measurements, these results (16 ± 4 kJ mol^{-1}) is close to the theoretical value. Hence the kinetics observed at the Pt microelectrode interface for both the membranes agree well with well-established mechanistic interpretations for ORR, which considers the electron transfer step in both oxide covered and oxide free Pt surface to be rate determining. However, the observed deviations do not completely rule out the possibility of the chemical step being rate determining. A more careful evaluation of this kinetics is necessary for making such a definitive distinction.

In the *lcd region* the SPES-40 and Nafion® 117 have close activation energies, in the hcd region however SPES-40 shows a lower value. Comparison of our data with previously reported values for Nafion® 117, shows a slightly lower value. Previously published results by Parathasarathy et al. [45–47] at 5 atm pressure was 75.24 and 27.5 kJ mol^{-1} in the low and high current density regions, respectively, corresponding to oxide covered and free Pt surfaces (lcd and hcd). Corresponding values reported at 3 atm by Beattie et al. [49] is 54.7 and 58.2 kJ mol^{-1}, respectively. Our values are 44.88

Table 3
Comparison of mass transport properties for various PEM systems studied as a function of temperature in the range 303–343 K, under conditions of 100% RH, 1 atm, O_2 pressure

T (K)	Nafion® 117				SPES-40			
	10^6D (cm^2 s^{-1})	10^6C (mol cm^{-3})	10^{12}DC (mol cm^{-1} s^{-1})	Volume of aqueous phase (%)	10^6D (cm^2 s^{-1})	10^6C (mol cm^{-3})	10^{12}DC (mol cm^{-1} s^{-1})	Volume of aqueous phase (%)
303	0.75	10.65	7.96	30.56	0.47	4.87	2.30	58.85
313	1.42	7.74	11.00	35.48	1.18	3.16	3.74	61.63
323	2.17	6.68	14.52	37.26	2.08	2.39	4.97	63.18
333	2.85	5.81	16.56	38.12	3.31	1.89	6.25	63.77
343	3.94	4.74	18.65	40.55	4.56	1.62	7.37	64.61

The reported values are the average of three separate experiments for each PEM system. The calculated volume of aqueous phase is also given as a function of temperature.

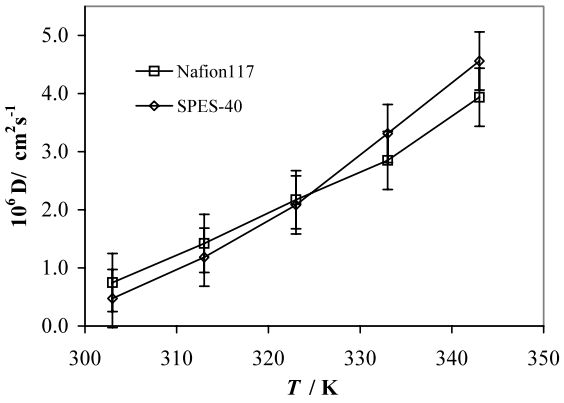

Fig. 7. Temperature T versus diffusion coefficient D of oxygen at Pt/PEM interface studied under conditions of 100% RH, temperature range 303–343 K, 1 atm O_2 pressure. (The error bars represent the limits of the range of behavior for each PEM system based on a set of three separate experiments.)

and 32.2 kJ mol^{-1} respectively at 1 atm pressure. There seems to be a good correlation with pressure, which agrees with the trend in the prior published data.

All data reported in Table 2, is the average of three separate experiments at each temperature for Nafion® 117 and SPES-40. Data in Figs. 2–5, represent examples of one of such data sets. The scatter in the data did not exceed 5%.

3.3. Determination of mass-transport parameters as a function of temperature by chronoamperometric method

Microelectrode technique had been successfully used to evaluate the diffusion coefficient (D), solubility (C) and permeability ($D \times C$) of O_2 in the polymer electrolyte membranes. Further, the Arrhenius behavior of these parameters was evaluated to provide the activation energy of diffusion and enthalpy of dissolution of oxygen in the membranes. Methodology for performing

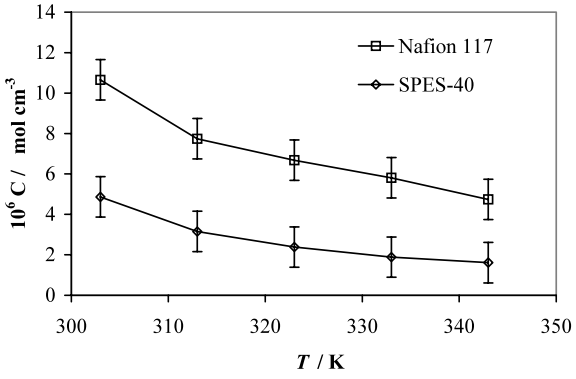

Fig. 8. Temperature T versus solubility of O_2 C at Pt/PEM interface studied under conditions of 100% RH, temperature range 303–343 K, 1 atm O_2 pressure. (The error bars represent the limits of the range of behavior for each PEM system based on a set of three separate experiments.)

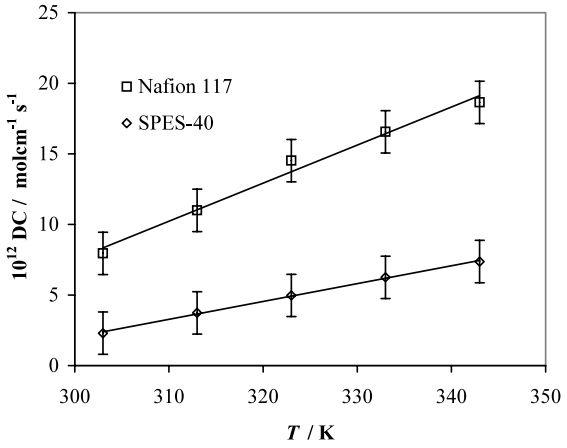

Fig. 9. Temperature T versus permeability of O_2 DC at Pt/PEM interface studied under conditions of 100% RH, temperature range 303–343 K, 1 atm O_2 pressure. (The error bars represent the limits of the range of behavior for each PEM system based on a set of three separate experiments.)

chronoamperometric measurements and data analysis are well established in literature [45,46,49].

Fig. 6 represents typical chronoamperometric plots for the reduction of O_2 at Pt/Nafion® 117 and Pt/SPES-40 interface under ambient O_2 pressure and at temperatures in the range 303–343 K. Each I versus $t^{-1/2}$ line was found to display well-defined linear behavior with a correlation coefficient ≥ 0.999. The mass transport results were given in Table 3 and illustrated in Figs. 7–9. Error bars in Figs. 7–9 represent scatter of data from three separate experiments. Data in Table 3, represents the average of these values. The principal features of this data can be summarized as following: (i) for all the membranes investigated, the diffusion coefficient D increases with temperature, the opposite trend is true for the solubility C, the overall permeability ($D \times C$), however shows an increasing trend with temperature. (ii) Over the temperature range studied, SPES-40 and Nafion® 117 have relatively close diffusion coefficients, though SPES-40 showed slightly higher values at the upper end of the temperature scale. Further, the slope of its variation with temperature was slightly higher than Nafion® 117. (iii) However, the oxygen solubility for Nafion® 117 is higher than SPES-40 in the entire temperature range investigated. (iv) The overall oxygen permeability for Nafion® 117 is greater than SPES-40. Further, the slope of its increase as a function of temperature is significantly higher than SPES-40.

Comparing our results of O_2 permeation with those reported earlier [46,49] leads to several interesting observations. The diffusion coefficient obtained for Nafion® 117 show reasonably close values with prior published data [46,49] in the same temperature range albeit at different pressures (5 [46] and 3 atm [49]). The solubility values were also close to earlier published values [46,49] though there were some differences due to

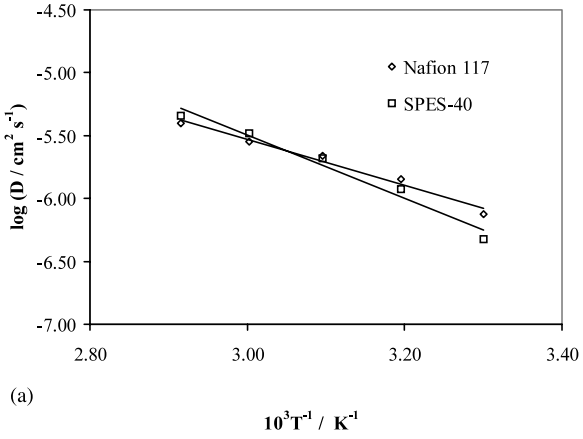

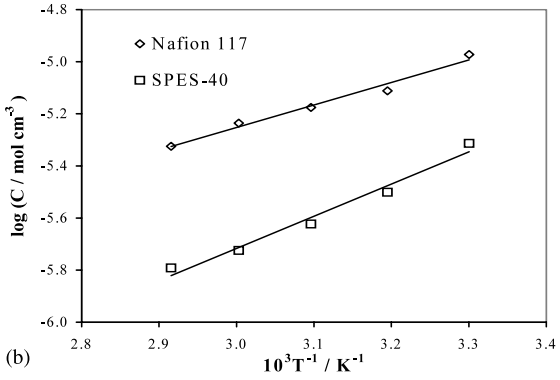

Fig. 10. Arrhenius plots of: (a) log D; and (b) log C versus 10^3 T^{-1} for various PEM membranes studied under conditions of 100% RH, temperature range 303–343 K, 1 atm O_2 pressure. (The values of D and C are average of three separate experimental data sets for each membrane system.)

different pressures used in these prior investigations [46,49].

Increase of diffusion coefficient and decrease of solubility with temperature in Nafion® 117 membrane mirror those reported earlier by Parthasarathy et al. [46] and Beattie et al. [49]. However, the above authors also demonstrated two linear regions in the Arrhenius plots for D and C with a break at 323 K. The first was in the range 303–323 K and second, 323–343 K, which led to separated values for activation energy for O_2 diffusion (E_d) and the enthalpy of dissolution of O_2 in the membrane (ΔH_s) corresponding to each temperature range. This behavior was not observed here. As illustrated in Fig. 10, log D and log C versus 10^3 T^{-1} plots for Nafion® 117 and SPES-40 membrane exhibit a linear response over the range of temperatures investigated (303–343 K) and therefore allowed unique E_d and ΔH_s values to be determined for each membrane. One possible reason for this may be due to the much lower O_2 pressure (1 atm) applied in this work as compared to those used in previous reports (5 [46] and 3 atm [49]). This is in agreement with the observation that in these prior reports [46,49] the two-region phenomenon at 3 atm was less distinct than that at 5 atm. In these prior reports [46,49], the break in Arrhenius behavior for both diffusion coefficient and solubility was explained on the basis of a similar break in the water uptake values as a function of temperature. This was reported by Parthasarathy et al. [46] and was used by Beattie et al. [49] in their explanations. Our data on the water uptake, did not show such a break, water uptake expressed as weight percent exhibited a monotonic increase with temperature (Table 4) for both Nafion® 117 and SPES-40. This agrees very well with prior published report by Hinatsu et al. [68]. This largely explains the continuously changing trends of the D and C for Nafion® 117 and SPES-40 as a function of temperature (Fig. 10). Water uptake for both Nafion® 117 and SPES-40, expressed in terms of variation of λ with temperature (Fig. 11) also exhibit the same behavior. Further study on SPES membranes as a function of pressure is expected to provide a better insight into this behavior.

Table 4
Water uptake values as a function of temperature in the range 298–373 K for various PEM membranes

T (°C)	Nafion 117		SPES-40	
	Water %	λ	Water %	λ
25	20	12.5	65	21.1
40	25	15.4	73	23.4
50	27	16.2	78	25.2
60	28	17.1	80	25.9
70	31	18.7	83	27
80	35	21.1	85	27.3
100	39	23.6	89	28.6

The data is reported both as water uptake in weight percent and in terms of $\lambda = [H_2O]/SO_3^-$.

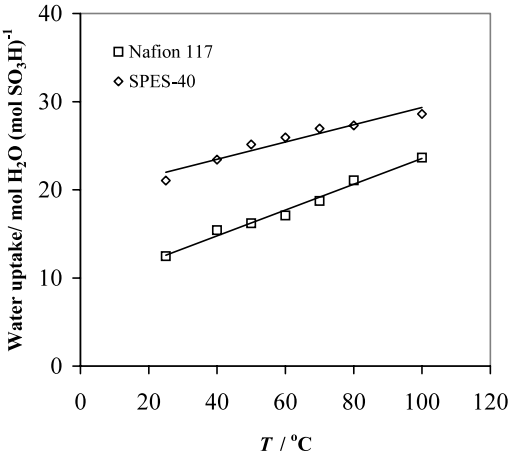

Fig. 11. Water uptake (expressed as number of moles of H_2O per SO_3^- group, λ) for various PEM membranes as a function of temperature.

It is well established that perfluorinated sulfonic acid membranes such as Nafion® 117 and other like membranes such as those from Asahi Chemicals (Aciplex® series) and Ballard (BAM® series) are phase

separated materials. It comprises of crystalline regions consisting of hydrophobic Teflon backbone and hydrophilic ionic domains made up of randomly attached pendant chains terminated with sulfonic acid groups. These are based on a wealth of earlier work such as those by Gierke et al. [69–71] which have established the formation of ionic clustering in these materials. The microstructure model, which has emerged, suggests the formation of inverted micelles with SO_3^- groups forming hydrated cluster embedded in fluorocarbon phase with diameters of 40–50 Å. As pointed out earlier [72], the water content in the membrane is determined by a combination of three processes: (i) water sorption by the membrane, which is controlled by its ion exchange capacity (number of ionic groups per unit weight); (ii) its electroosmotic drag coefficient, which is a function of its proton conductivity; and (iii) water diffusion caused by gradients in water activity. Recent AFM imaging studies [38] using a tapping mode have shown the existence of roughly two phases in the SPES membranes. The ionic cluster phase, comprising of hydrophilic sulfonic acid groups contain most of the associated water and non-ionic matrix phase, which may be assigned to the relatively hydrophobic aromatic backbone. It has also been pointed out earlier [45,46,48] that water acts as a plasticizer in Nafion® and hence increase of the water content enables increase in the diffusion coefficient of oxygen. Opposite is true for the solubility [45,46,48], where solubility of oxygen was determined by the fraction of the hydrophobic component in the membrane. Hence, shrinking of the hydrophobic phase leads to decrease in O_2 concentration, since O_2 tends to be more soluble in hydrophobic domains than in hydrophilic parts [73].

The role of water content as determined by its equivalent weight (EW) has been demonstrated earlier using a comparison of sulfonated α,β,β-trifluorostyrene (BAM®, Ballard, Canada) membranes with Nafion® 117 as well as an investigation on perfluorinated sulfonic acid membranes (Nafion® series as well as Aciplex membranes). A comparison of BAM-407 (EW = 407) with Nafion® 117 (EW = 1100) showed the expected result of higher diffusion coefficient and lower solubility (approximately four times) for BAM-407 relative to Nafion® 117 [49]. This was rationalized purely on the basis of water content in these membranes (87 wt.% for BAM-407 compared to 19 wt.% for Nafion® 117 at 50 °C) [49]. This is also evident when comparing this effect for a particular membrane as a function of EW or better water content. Prior results with BAM® (Ballard, Canada), DIAS® (DIAS Analytic, USA), Nafion® (Dupont, USA) and Aciplex® (Asahi chemicals, Japan) [48,51] show remarkable correlation with water content within each family of membranes. An estimation of this effect has been made using the extent of variation in the hydrophilic phase between membranes with different equivalent weights [48]. In this case a gravimetric density of 2.2 g cm^{-2} was assumed for the hydrophobic phase and 1.0 g cm^{-2} for the hydrophilic phase. For the hydrophobic phase the model system chosen was polytetrafluoroethylene (PTFE®). This is supported by earlier work by Ogumi [53], who found identical O_2 solubility and diffusion coefficient for dry Nafion® 125 and PTFE membranes. For the hydrophilic phase, the values reported in 1 M H_2SO_4 were used in the calculations. At 323 K, the D and C for O_2 in PTFE® is reported to be 0.35×10^{-6} cm^2 s^{-1} and 37×10^{-6} mol cm^{-3}. The corresponding values for O_2 in 1 M H_2SO_4 are 31×10^{-6} cm^2 s^{-1} and 5×10^{-6} mol cm^{-3}. The calculated values for the volume of aqueous phase are given in Table 3.

Our results comparing the SPES-40 and Nafion® 117 membranes show relatively close values of diffusion coefficients. This is in contrast to expectations based on ion exchange capacity (0.91 for Nafion® 117 vs. 1.72 for SPES-40) and the associated higher water uptake by SPES-40 (approximately double that of Nafion® 117). Hence despite higher water content, the O_2 diffusion in SPES membrane (D of SPES-40 $= 2.08 \times 10^{-6}$ cm^2 s^{-1}) was close to Nafion® 117 ($D = 2.17 \times 10^{-6}$ cm^2 s^{-1}). Comparison of the percent volume of aqueous phase near room temperature (30 °C) shows that SPES-40 has approximately double the value than Nafion® 117 (Table 3). However, the variation of percent aqueous volume with temperature is greater for Nafion® 117 as compared to SPES-40 (approximately double as shown in Table 3). There is little correlation however between the results on water uptake and percent volume of aqueous phase with corresponding results on diffusion coefficient (D).

Although the wealth of prior results seems to indicate that water plays a central role in determining the O_2 permeation in proton exchange membranes, its exact mechanism remains unclear and deserves further investigation. It is evident in this comparison that SPES membrane has a very different chemical structure as compared to Nafion® 117. The hydrophobicity of the aromatic backbone of SPES is not as strong as Nafion's perfluorinated backbone and the sulfonic acid functional group in SPES is somewhat less acidic than in Nafion®. Therefore, one may expect a less pronounced hydrophilic/hydrophobic separation in SPES as compared to Nafion® 117. Such behavior has been observed with the related sulfonated poly (ether-ether ketone) system using small angle X-ray scattering experiments[74]. As a result, one must use caution when comparing the mass transport characteristics of membranes with respect to difference in their water uptake alone. Difference in chemistry is also expected to play an important role.

Recent report based on results of AFM image analysis using tapping mode [38] shows some striking

Table 5
Comparison of O_2 permeation parameters (DC) at 323 K for various PEM systems studied

Membrane	IEC (meq g^{-1})	Water content (wt.%)	10^6D ($cm^2\ s^{-1}$)	10^6C (mol cm^{-3})	$10^{12}DC$ (mol $cm^{-1}\ s^{-1}$)	E_d (kJ mol^{-1})	ΔH_s (kJ mol^{-1})
Nafion 117	0.91	32	2.17	6.68	14.52	29.74	−14.35
SPES-40	1.72	64	2.08	2.39	4.97	40.36	−20.09

The reported values are the average of three separate experiments for each PEM system. (100% RH, 1 atm O_2).

findings concerning the morphologies of the ionic phases. For the SPES-40 membrane, the hydrophilic ionic domains are isolated and dispersed among the non-ionic matrix domains with an average of 25 nm diameter [38]. In contrast, the image of Nafion® 117, are reported to have significantly smaller hydrophilic ionic domains (about 10 nm) which tend to form continuous channels in structure [38]. Assuming that O_2 diffusion is predominantly related to the water. The well-connected channels between ionic domains of Nafion® 117 may form three-dimensional water network, which seems a more favorable transport pathway for O_2. As for SPES-40, despite the larger size of hydrophilic clusters, the water filled channels may be narrower or more branched with greater number of dead-ends, O_2 therefore gets blocked to a larger extent within SPES 40 thus leading to relatively smaller increase in the diffusion coefficient despite higher water content in the membrane.

In terms of solubility, comparison of data for Nafion® 117 and SPES-40, shows a much better correlation with water content. As shown in Table 5, Nafion® 117 (EW = 1100) has approximately 2.7 times higher solubility than SPES-40 at 50 °C, which agrees well with the approximately two fold lower water content of Nafion® 117. Fig. 8, shows the corresponding variation of solubility (C) with temperature. Here the trend follows the variation in the percent volume of aqueous phase (Table 3). Comparison with previous results for BAM® (Ballard, Canada) membrane with EW = 407, shows agreement with this trend. Here the comparison of the results at 3 atm, after pressure correction and adjustment to 1 atm, shows a correspondingly lower value of oxygen solubility in agreement with their higher water content. Even though reasonable correlation with water content is possible for SPES-40 membrane, in contrast to the corresponding characteristics with diffusion coefficient, the impact of their fundamental differences in chemistry cannot be ruled out.

The value of activation energy (E_d) for oxygen diffusion in Nafion® 117 determined using Arrhenius plot (Fig. 10(a)), is close to those published earlier [46,49]. As mentioned earlier, in our experiments we did not observe any sharp changes in the Arrhenius plots, which agrees well with our data of water uptake by Nafion® 117 (data for Nafion® 117 is also corroborated by that of Hinatsu et al. [68]) and SPES-40. In contrast to this, earlier published results have two values of E_d based on the temperature range 303–323 and 323–343 K. Our results with Nafion® 117, is close to earlier reported results in the 303–323 K range [46] (these results are however at elevated pressures, 5 [46], and 3 atm [49]). Comparison of the corresponding value for SPES-40 (Table 5) shows a much higher value for E_d (29.74 kJ mol^{-1} for Nafion® 117, compared to 40.36 kJ mol^{-1} for SPES-40). This higher activation energy can be explained on the basis of very different membrane morphology in SPES-40 as compared to Nafion® 117. This has been the subject of discussions in earlier sections above.

The value for enthalpy of dissolution, ΔH_s obtained from the corresponding Arrhenius plot of solubility (C), shows a slightly higher value for SPES-40 as compared to Nafion® 117. Comparison of the value for Nafion® 117 in the temperature range 303–323 K shows good agreement with earlier published results [46,49]. These results show a clear variation of ΔH_s with pressure, results at 5 atm report a value of −5.016 kJ mol^{-1} [46], those reported at 3 atm was −8.1 kJ mol^{-1} [49], our results at 1 atm, pressure (ambient) is −14.35 kJ mol^{-1}.

The positive slopes of the van't Hoff plots (log C vs. T^{-1}), indicate negative values for both ΔH_s and ΔS_s (from the intercept), these have implications in terms of the interaction of the aqueous and non-aqueous phases in the membrane and the effect of different membrane chemistry. A negative value for ΔS_s for oxygen dissolution can be regarded as an ordering process. As pointed out earlier, a negative value of oxygen dissolution can be expected based on negative entropy of dissolution in both the extreme ends of the phases of Nafion® (PTFE, non aqueous phase and H_2SO_4, aqueous phase). Therefore unique spatial arrangements of oxygen is expected between the aqueous and non-aqueous components of both Nafion® 117 and SPES-40. The higher values of ΔH_s and ΔS_s for SPES-40 as compared to Nafion® 117, indicates greater degree of spatial rearrangements during oxygen solubility in SPES-40. The exact mechanisms of these interactions however await a molecular modeling study.

Finally, the O_2 permeability (product of D and C) is more dependent on C, so membrane with higher solubility of oxygen tends to also have higher perme-

ability. From an overall perspective the SPES membranes has approximately three times lower O_2 permeability than Nafion® 117 (Table 5).

The lower solubility and permeability of oxygen in SPES-40, has very important implications for fabrication of practical membrane electrode assembly (MEA) using these materials. The choice of ionomer in the reaction layer of the electrode and its thickness will determine both the mass transport and activation overpotentials. Hence, a systematic evaluation of these oxygen permeability characteristics in these new class of membranes designed for elevated temperature operation is essential for designing improved PEM fuel cells.

4. Conclusions

Electrode kinetics and mass transport parameters were determined for Nafion® 117 and a sulfonated poly (arylene ether sulfone) membrane (SPES-40) at 1 atm O_2 pressure in a temperature range of 303–343 K.

Like Nafion® 117, Tafel plots at a Pt/SPES-40 membrane interface displayed two slopes corresponding to oxide covered and free Pt surface (low and high current density regions). The electrode kinetics of the SPES membrane was found to be in the same range as Nafion® 117.

For all the membranes investigated, the O_2 diffusion coefficient D increases with temperature, while the solubility C decreases. The overall permeability $D \times C$ however shows an increase as a function of temperature. SPES-40 and Nafion® 117 were found to have relatively close diffusion coefficients, despite the higher water uptake by SPES-40 (approximately twice the IEC). Oxygen solubility for Nafion® 117 was however significantly higher than SPES-40. These results were discussed in the context of water content and microstructure of the membranes. The conformations of water-filled channels connecting the hydrophilic ionic clusters appear to have important contributions in the process of O_2 diffusion. Chemistry of SPES membrane backbone appears to play a major role in determining the solubility of oxygen in these systems given its relatively lower hydrophobicity as compared to the perfluorinated backbone for Nafion®. From an overall perspective, the lower solubility of oxygen in the SPES membrane appears to effect the overall permeation of oxygen in this class of membranes.

Acknowledgements

The authors wish to acknowledge financial support from the Department of Energy, through a subcontract from Los Alamos National Laboratory. The authors would like to express their deep appreciation to Professor James McGrath at the Department of Chemistry, Virginia Polytechnic Institute and State University (Virginia Tech.) for providing SPES family of proton exchange membranes used in this work. The assistance of Richard C. Urian in the set up of the microelectrode assembly and the humidification control unit is deeply appreciated.

References

[1] O. Savadogo, J. New Mater. Electrochem. Syst. 1 (1998) 47.
[2] T.A. Zawodzinski, Jr., T.E. Springer, F. Uribe, S. Gottesfeld, Solid State Ionics 60 (1993) 199.
[3] F. Opekar, D. Svozil, J. Electroanal. Chem. 385 (1995) 269.
[4] Y. Sone, P. Ekdunge, D. Simonsson, J. Electrochem. Soc. 143 (1996) 1254.
[5] J.J. Sumner, S.E. Creager, J.J.A. Ma, D.D. DesMarteau, J. Electrochem. Soc. 145 (1998) 107.
[6] P.S. Kauranen, E. Skou, J. Appl. Electrochem. 26 (1996) 909.
[7] N. Jia, M.C. Lefebvre, J. Halfyard, Z. Qi, P.G. Pickup, Electrochem. Solid-State Lett. 3 (2000) 529.
[8] S.R. Samms, S. Wasmus, R.F. Savinell, J. Electrochem. Soc. 143 (1996) 1498.
[9] K.D. Kreuer, Solid State Ionics 97 (1997) 1.
[10] S. Malhotra, R. Datta, J. Electrochem. Soc. 144 (1997) L23.
[11] R.W. Kopitzke, C.A. Linkous, G.L. Nelson, Polymer Degradation Stability 67 (2000) 335.
[12] G. Alberti, M. Casciola, L. Massinelli, B. Bauer, J. Membr. Sci. 185 (2001) 73.
[13] M. Ise, K.D. Kreuer, J. Maier, Solid State Ionics 125 (1999) 213.
[14] S.D. Mikhailenko, S.M.J. Zaidi, S. Kaliaguine, Catalysis Today 67 (2001) 225.
[15] S.D. Mikhailenko, S.M.J. Zaidi, S. Kaliaguine, J. Polymer Sci., Part B: Polymer Phys. 38 (2000) 1386.
[16] S. Faure, N. Cornet, G. Gebel, R. Mercier, M. Pineri, B. Sillion, New Materials for Fuel Cell and Modern Battery Systems II, Proceedings of the International Symposium on New Materials for Fuel Cell and Modern Battery Systems, 2nd, Montreal, July 6–10, 1997 (1997) 818.
[17] R.W. Kopitzke, T.T. Steckler, B.D. Seurer, Abstracts of Papers, 223rd ACS National Meeting, Orlando, FL, United States, April 7–11, 2002 (2002) CHED.
[18] R.W. Kopitzke, B.D. Seurer, T.T. Steckler, Abstracts of Papers, 223rd ACS National Meeting, Orlando, FL, United States, April 7–11, 2002 (2002) CHED.
[19] F. Wang, M. Hickner, Q. Ji, W. Harrison, J. Mecham, T.A. Zawodzinski, J.E. McGrath, Macromolecular Symposia 175 (2001) 387.
[20] F. Lufrano, G. Squadrito, A. Patti, E. Passalacqua, J. Appl. Polymer Sci. 77 (2000) 1250.
[21] F. Lufrano, I. Gatto, P. Staiti, V. Antonucci, E. Passalacqua, Solid State Ionics 145 (2001) 47.
[22] R.W. Kopitzke, C.A. Linkous, H.R. Anderson, G.L. Nelson, J. Electrochem. Soc. 147 (2000) 1677.
[23] H.R. Allcock, M.A. Hofmann, C.M. Ambler, S.N. Lvov, X.Y. Zhou, E. Chalkova, J. Weston, J. Membr. Sci. 201 (2002) 47.
[24] M. Kawahara, M. Rikukawa, K. Sanui, N. Ogata, Solid State Ionics 136–137 (2000) 1193.
[25] M. Kawahara, M. Rikukawa, K. Sanui, Polym. Advanced Technol. 11 (2000) 544.
[26] J.M. Bae, I. Honma, M. Murata, T. Yamamoto, M. Rikukawa, N. Ogata, Solid State Ionics 147 (2002) 189.
[27] K. Miyatake, H. Iyotani, K. Yamamoto, E. Tsuchida, Macromolecules 29 (1996) 6969.

[28] R. Nolte, K. Ledjeff, M. Bauer, R. Muelhaupt, BHR Group Conf. Ser. Publ. 3 (1993) 381.
[29] R. Nolte, K. Ledjeff, M. Bauer, R. Muelhaupt, J. Membr. Sci. 83 (1993) 211.
[30] Y.S. Kim, F. Wang, M. Hickner, J.E. McGrath, T.A. Zawodzinski, Abstracts of Papers, 223rd ACS National Meeting, Orlando, FL, United States, April 7–11, 2002 (2002) POLY.
[31] S.R. Brankovic, J.X. Wang, R.R. Adzic, Electrochem. Solid-State Lett. 4 (2001) A217.
[32] M.A. Hickner, F. Wang, Y.S. Kim, B. Pivovar, T.A. Zawodzinski, S. McGrath, Preprints of Symposia—American Chemical Society, Division of Fuel Chemistry 46 (2001) 459.
[33] R.E. Kesting, Synthetic Polymeric Membranes. A Structural Perspective, 2nd ed, 1985.
[34] M.R. Pereira, J. Yarwood, J. Chem. Soc., Faraday Trans. 92 (1996) 2731.
[35] F. Wang, Y. Kim, M. Hickner, T.A. Zawodzinski, J.E. McGrath, Polymeric Mater. Sci. Eng. 85 (2001) 517.
[36] M. Ciureanu, H. Wang, J. New Mater. Electrochem. Syst. 3 (2000) 107.
[37] F. Wang, T. Glass, X. Li, M. Hickner, Y. Kim, J. McGrath, Polymer Preprints (American Chemical Society, Division of Polymer Chemistry) 43 (2002) 492.
[38] F. Wang, M. Hickner, Y.S. Kim, T.A. Zawodzinski, J.E. McGrath, J. Membr. Sci. 197 (2002) 231.
[39] T.E. Springer, M.S. Wilson, S. Gottesfeld, J. Electrochem. Soc. 140 (1993) 3513.
[40] A.J. Appleby, J. Electrochem. Soc. 117 (1970) 328.
[41] A.J. Appleby, J. Electrochem. Soc. 117 (1970) 641.
[42] S. Gottesfeld, I.D. Raistrick, S. Srinivasan, J. Electrochem. Soc. 134 (1987) 1455.
[43] K.L. Hsueh, H.H. Chang, D.T. Chin, S. Srinivasan, Proc.-Electrochem. Soc. 84-12 (1984) 558.
[44] W.E. O'Grady, E.J. Taylor, S. Srinivasan, J. Electroanal. Chem. Interfacial Electrochem. 132 (1982) 137.
[45] A. Parthasarathy, C.R. Martin, S. Srinivasan, J. Electrochem. Soc. 138 (1991) 916.
[46] A. Parthasarathy, S. Srinivasan, A.J. Appleby, J. Electrochem. Soc. 139 (1992) 2530.
[47] A. Parthasarathy, S. Srinivasan, A.J. Appleby, C.R. Martin, J. Electrochem. Soc. 139 (1992) 2856.
[48] F.N. Buechi, M. Wakizoe, S. Srinivasan, J. Electrochem. Soc. 143 (1996) 927.
[49] P.D. Beattie, V.I. Basura, S. Holdcroft, J. Electroanal. Chem. 468 (1999) 180.
[50] V.I. Basura, P.D. Beattie, S. Holdcroft, J. Electroanal. Chem. 458 (1998) 1.
[51] V.I. Basura, C. Chuy, P.D. Beattie, S. Holdcroft, J. Electroanal. Chem. 501 (2001) 77.
[52] Z. Ogumi, T. Kuroe, Z. Takehara, J. Electrochem. Soc. 132 (1985) 2601.
[53] Z. Ogumi, Z. Takehara, S. Yoshizawa, J. Electrochem. Soc. 131 (1984) 769.
[54] Y.M. Tsou, M.C. Kimble, R.E. White, J. Electrochem. Soc. 139 (1992) 1913.
[55] A.T. Haug, R.E. White, J. Electrochem. Soc. 147 (2000) 980.
[56] T. Lehtinen, G. Sundholm, S. Holmberg, F. Sundholm, P. Bjornbom, M. Bursell, Electrochim. Acta 43 (1998) 1881.
[57] T. Sakai, H. Takenaka, N. Wakabayashi, Y. Kawami, E. Torikai, J. Electrochem. Soc. 132 (1985) 1328.
[58] T. Sakai, H. Takenaka, E. Torikai, J. Electrochem. Soc. 133 (1986) 88.
[59] K. Broka, P. Ekdunge, J. Applied Electrochem. 27 (1997) 117.
[60] J.M.D. Rodriguez, J.A.H. Melian, J.P. Pena, J. Chem. Edu. 77 (2000) 1195.
[61] T. Biegler, D.A.J. Rand, R. Woods, J. Electroanal. Chem. Interfacial Electrochem. 29 (1971) 269.
[62] S. Holdcroft, V.I. Basura, P.D. Beattie, Book of Abstracts, 217th ACS National Meeting, Anaheim, Calif., March 21–25, 1999, MSE.
[63] J. Giner, J. Electrochem. Soc. 111 (1964) 376.
[64] A. Damjanovic, V. Brusic, Electrochim. Acta 12 (1967) 615.
[65] A. Damjanovic, M.A. Genshaw, Electrochim. Acta 15 (1970) 1281.
[66] J.O.M. Bokris, A. Gochev, J. Electroanal. Chem. Interface Chem. 214 (1986) 655.
[67] D.B. Sepa, M.V. Vojnovic, L.M. Vracar, A. Damjanovic, Electrochim. Acta 29 (1984) 1169.
[68] J.T. Hinatsu, M. Mizuhata, H. Takenaka, J. Electrochem. Soc. 141 (1994) 1493.
[69] T.D. Gierke, G.E. Munn, F.C. Wilson, J. Polymer Sci., Polymer Phys., Ed 19 (1981) 1687.
[70] W.Y. Hsu, T.D. Gierke, Macromolecules 15 (1982) 101.
[71] W.Y. Hsu, T.D. Gierke, J. Membr. Sci. 13 (1983) 307.
[72] S.J. Paddison, T.A. Zawodzinski, Jr., Solid State Ionics 113–115 (1998) 333.
[73] P.C. Lee, M.A.J. Rodgers, J. Phys. Chem. 88 (1984) 4385.
[74] K.D. Kreuer, J. Membr. Sci. 185 (2001) 29.